Harnessing Organic Ligand Libraries for First-Principles Inorganic Discovery: Indium Phosphide Quantum Dot Precursor Design Strategies

Harnessing Organic Ligand Libraries for First-Principles Inorganic Discovery: Indium Phosphide Quantum Dot Precursor Design Strategies

Jeong Yun Kim[I], Adam H. Steeves[I], and Heather J. Kulik[I]*

[I]*Department of Chemical Engineering, Massachusetts Institute of Technology, Cambridge, MA 02139*

ABSTRACT: Indium phosphide quantum dots (QDs) represent promising replacements for more toxic QDs, but InP QD production lags behind other QD materials due to limited understanding of how to tune InP QD growth. We carry out a first-principles, computational screen of the tuning of In carboxylate precursor chemistry to alter the kinetics of elementary steps in InP QD growth. We employ a large database normally used for discovery of therapeutic drug-like molecules to discover design rules for these inorganic complexes while maintaining realism (i.e., stable, synthetically accessible substituents) and providing diversity in a 210-molecule test set. We show the In-O bond cleavage energy, which is tuned through ligand functionalization, to be a useful proxy for In-P bond formation energetics in InP QD synthesis. Energy decomposition analysis on a 32-molecule subset reveals that lower activation energies correlate to later transition states, due to stabilization from greater In-P bond formation and more favorable reaction energetics. Our simulations suggest that altering ligand nucleophilicity tunes the reaction barrier over a 10 kcal/mol range, providing the conjugate acid's pK_a as an experimental handle to lead to better control of growth conditions and to improve synthesized InP QD quality. Importantly, these trends hold regardless of phosphorus precursor chemistries and in longer chain length ligands typically used in synthesis.

1. Introduction

Colloidal quantum dots (QDs) have attracted intense attention for their unique size-

dependent electronic and optical properties[1-2], relevant for applications in photovoltaics,[3-5] light-emitting diodes,[6-7] and biological imaging.[8-9] Well-known cadmium selenide (CdSe)-based QDs exhibit controllable sizes[10-11] and light emission throughout the entire visible range[12], but the high toxicity of cadmium[13] motivates the search for non-toxic replacements. Indium phosphide (InP) QDs represent promising alternatives to CdSe-based QDs due to lack of intrinsic toxicity[14-15] and broader emission profiles.[16-17] Current InP QD synthesis approaches have failed to obtain optimal InP QD size distribution and high quantum yields comparable to CdSe-based QDs, despite ongoing experimental efforts to understand the QD formation mechanism[18-23] and tune the growth process.[24-25] Nucleation models that work for more ionic II-VI compounds fail for III-V QDs[26]. Further, the need for high temperatures, reactive phosphorus precursors, and long reaction times for the synthesis of more covalent InP QDs makes control of size distributions challenging.[27]

First-principles simulations can provide valuable insight into the chemistry of quantum dots and their precursors. Simulations have been widely used to understand and improve the growth mechanism[28-29] of II-VI and IV-VI QDs (e.g., CdSe, PbSe and PbS) or understanding ligand exchange in coinage metal QDs[30-33]. Although the properties of amorphous[34], bulk[35-37], and confined InP[34, 38-41] have been studied in detail, less work has been carried out to understand their growth mechanisms. Recently, we used a combined *ab initio* molecular dynamics (AIMD) and reaction pathway analysis approach to discover the kinetics of early stage growth in InP QDs.[42] Through AIMD, we observed the formation of the earliest stage of InP QDs with an indium rich surface in excellent structural agreement with recently characterized InP magic sized clusters[19, 43-44]. We also identified indium carboxylate precursor chemistry (i.e., In-O bond dissociation energetics) to play an essential role in determining kinetic barriers that necessitate high temperatures in InP QD synthesis.

Despite this essential role of the indium precursor, focus has remained on the highly reactive nature of common phosphorus precursors (e.g., tris(trimethylsilyl)-phosphine, ($P(SiMe_3)_3$) employed for the growth of InP QDs, as they are believed to be the main cause of the poor size QD distribution, in analogy to other classes of QDs.[14, 23] Indeed, experimental effort has been

aimed at identifying phosphorus precursors with slower conversion rate to prevent fast depletion at high temperatures[24, 45-47], but this approach has proven ineffective in improving QD size distributions.[26] The challenges encountered in adjustment of group-V precursor chemistry to enhance the quality of QDs[26] and earlier successes with improving yield through indium precursor tuning[19, 48-49] motivate the reconsideration of altering indium precursor chemistry to tune In-P bond formation. Six-coordinate indium carboxylates[50-52] are widely employed in InP QD synthesis. Although carboxylate chain length is known to be important to synthetic outcomes[14, 48] and the form of the indium complex (i.e., phosphonate instead of carboxylate) has been shown to produce altered properties[19], subtle variation in ligand chemistry has not been widely pursued as a mechanism to tune early stage growth kinetics.

In this work, we introduce a first-principles computational discovery approach to identify design strategies for the chemistry of indium carboxylate precursors to tune early-stage InP QD growth kinetics. We repurpose large libraries[53] and molecular similarity metrics, normally employed in organic molecule design, in an inorganic discovery toolkit[54] to identify new indium precursor candidates. A similar repurposing approach has very recently been demonstrated[55] in experimental screening of transition metal catalysts. Through our computational approach, we identify relationships between indium carboxylate chemistry and In-P bond formation energetics that can help guide alternative recipes for InP QD synthesis. In Section 2, we summarize the Computational Details used in our study. In the Results and Discussion (sec. 3), we present the approach and results of our screen, a detailed analysis of the source of changes in energetics, and provide strategies for implementing suggested design elements in experimental synthesis. Finally, we summarize our Conclusions in section 4.

2. Computational Details

Density functional theory (DFT) single point energies and geometry optimizations were carried out with the B3LYP[56-58] hybrid exchange-correlation functional with the VWN1-RPA form for the LDA VWN[59] component of LYP[56] correlation, as implemented in TeraChem[60-61]. The composite LACVP* basis set was used, which consists of the Los Alamos effective core

potential (LANL2DZ)[62] for indium atoms and the 6-31G* basis set for the remaining atoms. Larger basis sets yielded comparable results on representative cases (Supporting Information Table S1). Geometry optimizations used the L-BFGS algorithm in Cartesian coordinates with the DL-FIND[63] interface to TeraChem. Default thresholds were used, which correspond to 4.5×10^{-4} hartree/bohr for the maximum gradient and 1.0×10^{-6} hartree for the change in total energy between steps. All reported energies are obtained in the gas phase, as tests with implicit solvent using the dielectric constant of solvents used in experimental conditions (ε=2) yielded comparable results (Supporting Information Table S2). Initial structures for geometry optimizations in the high-throughput screen were generated in both bidentate and monodentate structures using a template ($In(Ac)_3$) structure (Supporting Information Figure S1).

Using In-P bond formation pathways in the reaction of indium acetate precursors with phosphine we obtained previously,[42] we generated initial guesses for intermediates and transition states of modified precursors with the molSimplify toolkit.[54] We preserved the central core reacting In, P, H, and surrounding carboxylate atoms, which acted as a template for the placement of functionalized ligands. This structure building approach is the same as outlined for our previous efforts in screening functionalized ferrocenium complexes.[64] Constrained optimizations, with the central core atoms fixed, were carried out on these structures to obtain a good initial guesses of transition states for subsequent transition state searches. For larger phosphorus precursors ($P(XH_3)_3$, where X = Ge or Si), we first performed a nudged elastic band (NEB) calculation[65-66] for P-X bond dissociation in TeraChem. The highest energy image from NEB calculation was extracted for further refinement.

Transition states were obtained with partitioned rational function optimization (P-RFO)[67] at the B3LYP/LACVP* level of theory using Q-Chem 4.2[68]. All transition states were characterized with vibrational frequency analysis to confirm a single imaginary frequency corresponding to P-H bond dissociation. For intercomplex In-P bond formation, a second imaginary frequency with zero intensity and a value of < 30i cm^{-1} was typically detected, likely due to soft modes in the weakly bound intercomplex structures. Activation energies (E_a) for the

intracomplex and intercomplex pathways were determined with respect to the energies of an isolated bidentate-coordinated In precursor and a two-In precursor sharing a single bridging carboxylate, respectively. Entropic corrections were found to be comparable across tuned species and their inclusion did not alter observed trends over representative cases, so we exclude them due to the ambiguity in their calculation for the larger intercomplex species with soft modes (Supporting Information Figure S2).

Electrostatic potentials were calculated on select intermediates using default options in Q-Chem. Isodesmic pK_a calculations from first-principles are highly sensitive to the solvation method employed, yielding too large variations across the molecules studied (Supporting Information Table S3). Instead, the pK_a values of carboxylic acid group of selected compounds were predicted from the Calculator Plugins to MarvinSketch[69]. The algorithm uses an empirical model of the partial charge distribution, polarizability, and structure-specific factors to predict the acid dissociation constant.

3. Results and Discussion

3a. Screening Approach

Previous work from our lab suggested[42] that the chemistry of the indium carboxylate precursor is the primary determinant of the reaction energetics for In-P bond formation during InP QD synthesis. Specifically, if an In precursor structure with one monodentate-coordinated carboxylate reacts with a phosphorus precursor, the reaction from a higher energy intermediate state is nearly barrierless (Figure 1). The comparable energetics of the formation of the monodentate structure and the cleavage of the In-O bond required in the transition state suggests that the activation energy for In-P bond formation is strongly determined by In-O bond cleavage energetics. This observation contrasts with the emphasis that has been placed on tuning the phosphorus precursor to control kinetics.[26] Reducing the barrier for In-P bond formation through careful precursor selection could enable low temperature synthesis routes for more controlled growth and higher quality QDs. Other steps critical to QD synthesis include the release of precursors from intermediate-sized clusters[43, 70], which would involve the same bond cleavage and

formation events represented by Figure 1 but in likely more complex structures.

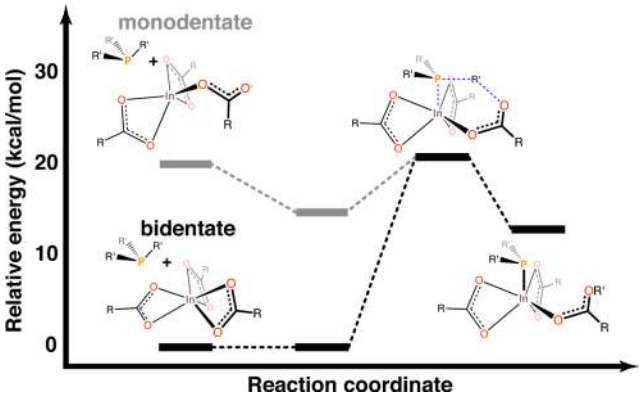

Figure 1. Schematic of intracomplex In-P bond formation reaction energetics for bidentate indium precursors compared to a case in which one carboxylate is already monodentate. The reactants correspond to separately calculated precursor energetics, whereas the second step is their computed binding energies in a reactant configuration. This latter binding energy is higher in the monodentate than bidentate case.

We carried out a systematic screen to discover functionalizations of carboxylate ligands that can tune In-O bond cleavage energetics. Using the molSimplify code,[54] candidate carboxylate-containing molecules were obtained from the ChEMBL-19[53] database that contains over 1.4 million unique molecules, of which over 110,000 molecules contain a single carboxylic acid or carboxylate functional group. The primary use case for such a database is for the discovery of organic molecules that can serve as therapeutic drugs, but it also represents a potential source for computational inorganic complex design. Indeed, the value of searching synthetically accessible molecules to repurpose them for applications in transition metal catalysis has been very recently appreciated in experimental efforts.[55] We select these molecules as our design space in order to ensure realism in our computational discovery efforts. This approach is to our knowledge the first use of such a database in computational inorganic complex design.

Since it would not be possible to directly screen that many molecules using first-principles techniques, we created a data set from two ligand screens: 1) all database molecules (110) with 15 or fewer atoms including the carboxylate and 2) the 100 most diverse 16-30 atom molecules in the database, as determined by a molecular similarity algorithm.[71-72] The database search module in molSimplify excludes fragmented molecules and strips counterion salt atoms. We also limit elemental composition to first row (C, H, N, O) organic elements and halogens (F, Cl, Br,

I). We previously found[42] the commonly employed indium myristate ($In(My)_3$) precursor,[24-25] which contains thirteen-carbon alkane chain ligands terminating in a carboxylate group, to have comparable monodentate-bidentate (m-b) energetics (19 kcal/mol) as compared to the much smaller indium acetate ($In(Ac)_3$) (20 kcal/mol). Therefore, we expect these 30-atom-or-smaller ligands to span the most relevant tuning strategies for indium precursors. The complete list of ligands and their structural characteristics is provided in Supporting Information Table S4, and 2D representations of all ligands are provided in Supporting Information Figures S3-S8.

We geometry optimized each indium-containing precursor in monodentate (m) and bidentate (b) structures to obtain their relative energies, $\Delta E_{m\text{-}b}$ (Figure 2). Negative relative energies of the monodentate configuration suggest the presence of an additional interaction that stabilizes monodentate structures more than bidentate structures, such as inter-ligand hydrogen bonding. No correlation between relative energetics and molecular weight of the constituent ligands was observed (Supporting Information Figure S9), ruling out steric factors as the driving force of the energetic spread. Steric bulk of ligands, however, could impact later stages of growth by impeding formation of previously observed densely packed ligands on magic-sized clusters[44] or altering kinetics of how clusters act as a source for precursor ligands[70].

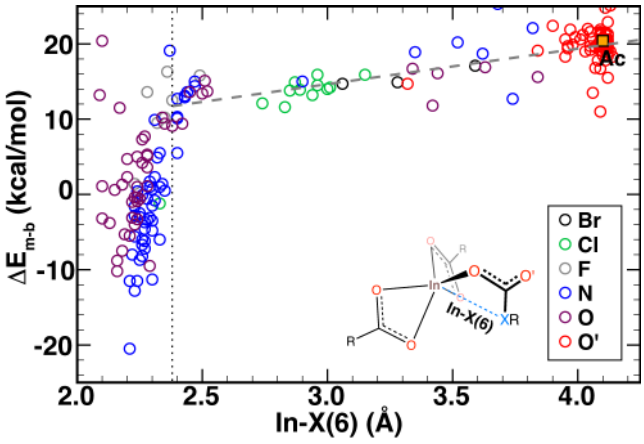

Figure 2. Relative monodentate and bidentate indium-carboxylate energetics ($\Delta E_{m\text{-}b}$ in kcal/mol) for 210 candidate structures plotted against the distance to the closest sixth coordinating atom in the monodentate structure (In-X(6) in Å, schematic shown in inset). O' refers to the original carboxylate oxygen if no other atom is closer. The $In(Ac)_3$ reference energy is shown with a filled orange square and annotated 'Ac'. A trendline (dashed, gray) is fit to data outside a 2.37 Å cutoff corresponding to 10% larger than the covalent In-O bond distance.

We observe a stronger energetic correlation with the shortest distance between the indium center and an additional atom (X(6)) outside of the five explicitly coordinated carboxylate oxygens (In-X(6)) in the monodentate configuration (Figure 2). This effect could be due to: i) reformation of the original covalent bond (i.e., a monodentate starting structure that optimizes to a bidentate structure) or introduction of a new sixth bond to a different functional group, ii) a favorable non-bonded interaction between indium and the adjacent species that is too long to be considered a full covalent bond, or iii) indirect effects on the carboxylate ligand that are strongest when the functional group atom is close to the carboxylate. With the goal of tuning In-P bond formation, it is unfavorable to have a fully six-coordinate indium (case i) because it will not be reactive toward a phosphorus precursor. The latter two cases are expected to favorably influence the In-P bond formation energetics, although we note that for case ii interactions formed in the monodentate geometry (Figure 2) are not necessarily likely to be preserved in a transition state structure (Figure 1).

We qualitatively designate covalent bond reformation (case i) as distances up to 10% larger (2.37 Å) than a typical 2.13 Å In-O bond, which occurs in 81 of the 210 screened structures (Supporting Information Table S4). For the remaining 129 molecules, $\Delta E_{m\text{-}b}$ energies range from 5 to 25 kcal/mol. A best-fit line for these 129 molecules has a slope of 4.7 kcal/mol·Å^{-1} (R^2=0.63), which suggests that a 1.7 Å reduction in the closest X(6) coordinating distance should stabilize the monodentate structure by 8 kcal/mol through case ii or iii effects. Halogen substitution (e.g., Cl, Br, and F) at the carboxylate α- or β-carbon make up a large portion of the lowest $\Delta E_{m\text{-}b}$ structures in our screen (Supporting Information Figure S10). Ligands with flexible oxygen-containing functional groups predominate in the case i set, but oxygen- or nitrogen-containing functional groups constrained in planar or ring structures also have favorable energetics (Supporting Information Figure S10 and Table S4).

Outliers from the nearest-atom distance to energy correlation are typically due to hydrogen bonds that stabilize the monodentate structure over the bidentate structure. For example, a point with $\Delta E_{m\text{-}b}$ = 10 kcal/mol but no nearby sixth interaction forms a hydrogen bond between the

accessible monodentate oxygen of the carboxylate and an -NH group on a neighboring ligand. Unexpectedly high $\Delta E_{m\text{-}b}$ energies despite the presence of short In-X(6) distances are also observed due to monodentate orientations disrupting favorable hydrogen bonding present in the bidentate structures.

3b. Correlating Bond Cleavage to Activation Energies

We selected 32 representative ligands from our original screen to identify if In-O bond cleavage energetics are a good proxy for reduced In-P bond formation activation energies, E_a, in quantum dot synthesis (Supporting Information Figure S11). These 32 precursors fall outside the covalent cutoff distance and have $\Delta E_{m\text{-}b}$ values ranging from 11 to 23 kcal/mol (Supporting Information Table S5). Our motivation for correlating $\Delta E_{m\text{-}b}$ to E_a is to relate the former equilibrium property that may be rapidly screened to the latter transition state property that requires more computational effort to compute. Alternatively, we could have considered a structural descriptor of the monodentate structure (i.e., In-X(6) in Figure 2), but that property overemphasizes case ii effects that can be preserved in the monodentate structure but not in the TS (see Figure 1). In previous work[42], we studied two pathways for In-P bond formation: i) the intracomplex, and ii) the intercomplex pathway. We found the intercomplex pathway, which requires multiple indium precursor species, to be energetically more favorable, an observation consistent with experimental recipes that require excess indium for synthesis[14]. However, we first examine functionalization effects on the intracomplex pathway (see Figure 1), due to its simplicity, in order to validate our hypothesis that activation energies (E_a) and In-O bond cleavage energies ($\Delta E_{m\text{-}b}$) are correlated.

A good correlation (R^2=0.58) is observed between intracomplex E_a and the $\Delta E_{m\text{-}b}$ values (Figure 3). The slope of the best-fit line indicates that a 10 kcal/mol reduction in $\Delta E_{m\text{-}b}$ value from the acetate reference reduces E_a by 4.9 kcal/mol. One outlier ($\Delta E_{m\text{-}b}$=22.1 kcal/mol, E_a=14.6 kcal/mol) is excluded from this trendline due to hydrogen bonding disrupted in the monodentate structure but preserved in the TS and bidentate structures (see Supporting Information Table S5).

The partial benefit and only moderate correlation of R^2=0.58 observed in E_a reduction compared to In-O bond cleavage may be understood by recalling differences in monodentate and transition state (TS) structures (see Figures 1 and 2). Stabilizing noncovalent interactions (case ii) preserved in the monodentate structure may be absent from the TS. Thus, In-O bond cleavage energetics provide a compromise as an efficient target for computational screening: they likely capture effects present in both the TS and monodentate structures but may overemphasize beneficial case ii interactions absent from the TS. Comparing all 32 cases, functional groups located beyond the β-carbon have a negligible effect on In-P bond formation energetics, validating our screening choice to emphasize carboxylate-proximal functional groups (Supporting Information Table S5).

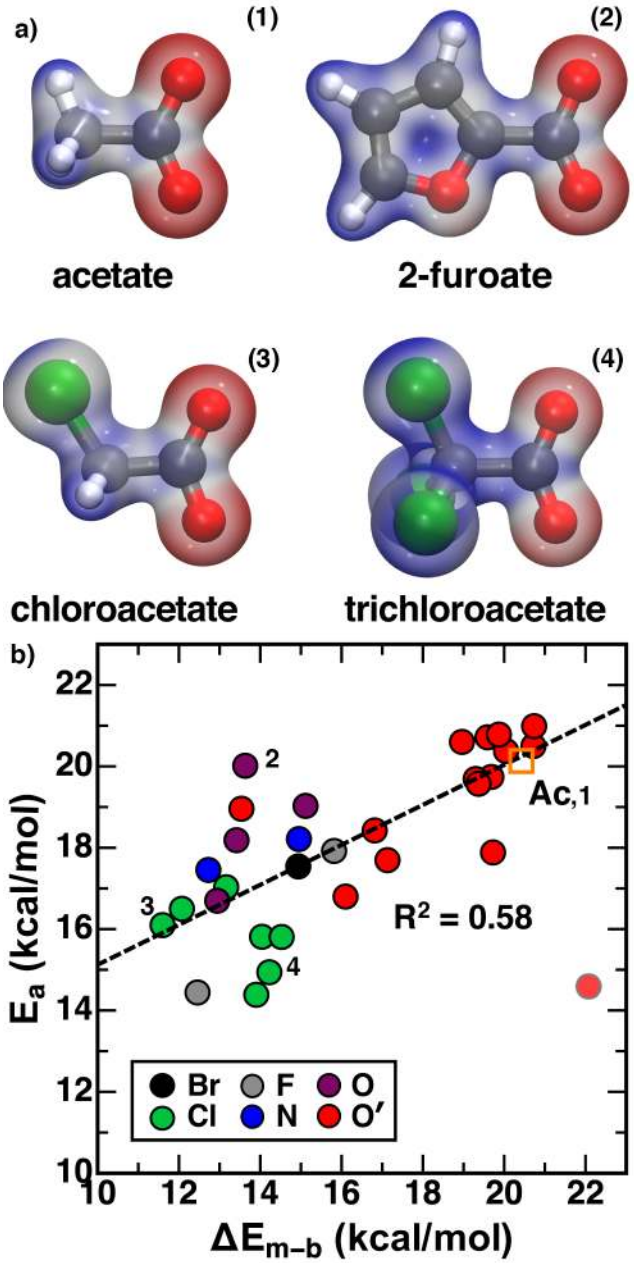

Figure 3. (a) Electrostatic potential (ESP) surfaces of four representative carboxylate ligands. The ESP is mapped on an electronic density isosurface of 0.05 e with a color scale ranging from red (electronegative regions, -0.25 e) to blue (electropositive regions, 0.05 e). (b) Activation energies (E_a, in kcal/mol) of the intracomplex pathway for In-P bond formation plotted against the relative monodentate and bidentate indium-carboxylate energetics (ΔE_{m-b}, in kcal/mol) for 32 carboxylate ligands. The data are colored by the closest atom to In in the monodentate carboxylate, as indicated in the inset legend, and the compounds shown in (a) are labeled accordingly. The $In(Ac)_3$ reference is shown with an empty orange square annotated 'Ac'. A trendline (dashed, black) is fit to data, excluding one outlier distinguished by gray outline on the symbol.

Ligands that are multiply halogenated at the α-carbon generally lie below the trendline and

have the lowest activation energies. Since the trichloroacetate case (4 in Figure 3) has a lower activation energy than chloroacetate (3 in Figure 3) but the same nominal sixth interaction, these results suggest that case ii effects are not dominating. In contrast, several oxygen- and nitrogen-containing compounds have low In-O bond cleavage energies but relatively high intracomplex E_a values (see 2-furoate in Figure 3). Comparison of monodentate and TS structures for 2-furoate reveals a favorable short In-O interaction in the former that is not preserved in the latter (structures provided in the Supporting Information). Examining the electrostatic potential of representative structures reveals a less electron-rich carboxylate oxygen in trichloroacetate, one of the below-trend cases. Thus, it appears that lower electron density at the carboxylate oxygen (i.e., case iii indirect interactions) is a likely explanation for cases where both In-O bond cleavage and In-P bond formation activation energies are reduced (see Sec. 3c). Indeed, replacement of two carbon atoms in the five-membered ring of 2-furoate with electron withdrawing nitrogen atoms (i.e., 3-methyl-1,2,4-oxadiazole-5-carboxylate) produces an E_a value (16.7 vs. 20.0 kcal/mol for 2-furoate) much closer to the trendline (see Figure 3).

3c. Rationalizing Energetic Trends with Functionalization

In order to identify the mechanism of TS stabilization for functionalized indium precursors, we use the activation strain model (ASM)[73-74] to decompose activation energies into contributions from substituent fragments. The ASM approach has been successfully applied in the fields of catalysis[75-77] and organic chemistry[78-79] to analyze TS structures. Within the ASM method, the strain associated with each reacting fragment is defined in terms of the difference in energy of the isolated fragment (e.g., at the transition state) versus in a reference reactant state (Figure 4). Thus, the activation energy is the sum of the strain in the two reacting fragments and the interaction energy:

$$E_a = E_{\text{strain-In}} + E_{\text{strain-P}} + E_{\text{int}} \quad (1)$$

For indium acetate and phosphine, an intracomplex In-P bond formation E_a of 20 kcal/mol is decomposed using eqn. 1 into 40 kcal/mol strain in the indium precursor, 24 kcal/mol strain in

the phosphorus precursor, and a corresponding -44 kcal/mol interaction energy between the deformed precursors in the transition state. Surprisingly, the strain energy in the indium precursor is larger than In-O bond cleavage (21 kcal/mol) due to substantial additional ligand distortion. The phosphorus precursor strain is derived from P-H* bond stretching and distortion of the phosphorus cone angle[80]. The interaction energy is derived from formation of the In-P and $H^{\cdot}$-O^{-} bonds in the TS (Figure 4).

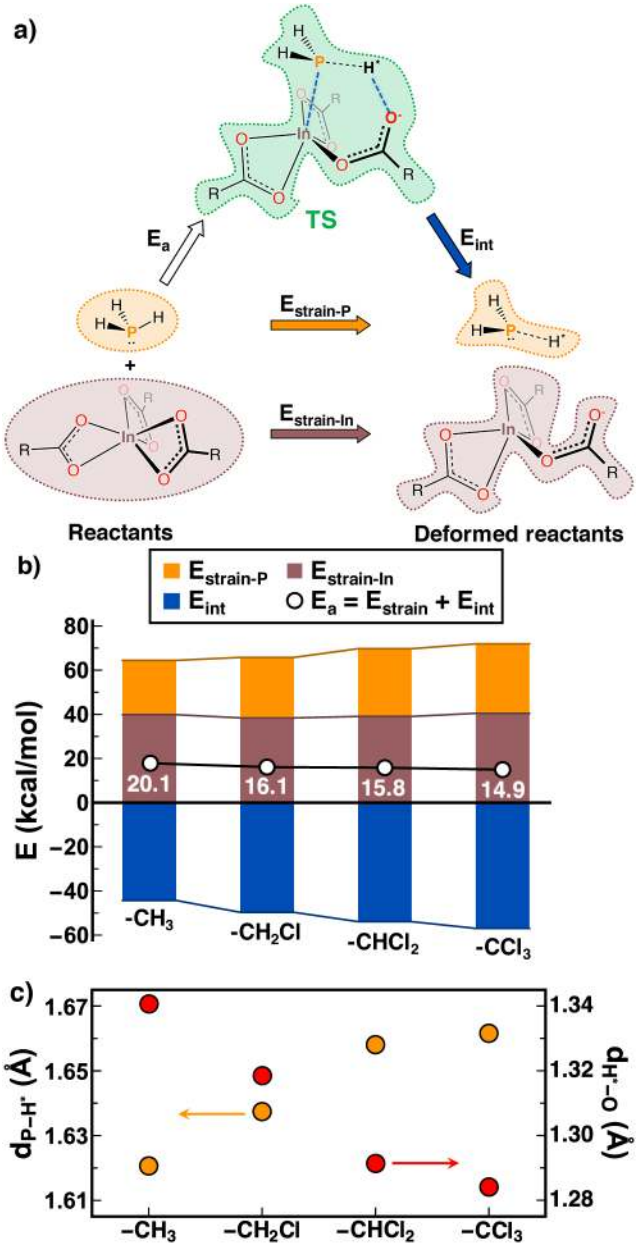

Figure 4. (a) Illustration of the activation strain model (ASM) for the intracomplex In-P bond

formation pathway between indium and phosphorus precursors. The E_a and three ASM decomposition energy components (interaction, phosphorus precursor strain, and indium precursor strain energies) are shown between corresponding structures. (b) Stacked bar graph of the activation (white circle), interaction (blue), indium precursor (brown), and phosphorus precursor (orange) strain energies of TS structure are shown for the acetate and three Cl-functionalized carboxylate ligands. (c) The bond distances between P-H* (orange) and H*-O$^-$ (red) of the TS structures are shown for the same four carboxylate ligands indicated in (b).

The ASM analysis is useful to identify functionalization effects, and we focus on mono- di- and tricholoro-acetate indium precursors due to their increasingly low intracomplex pathway E_a values through case iii effects (Figure 4). For increasingly chlorinated ligands, $E_{strain\text{-}In}$ remains constant and comparable to the indium acetate case at around 40 kcal/mol. The $E_{strain\text{-}P}$ increases from 27 to 31 kcal/mol, due to increasing P-H* bond distances in the transition state (Figure 4c). Lower overall E_a is then explained by increasing E_{int} from -50 to -57 kcal/mol due to increased In-P and H$^-$-O$^-$ bond formation without any In precursor strain penalty (Figure 4c).

The increase in strain in the phosphorus precursor for TSes with functionalized indium precursors can arise from two sources: i) the extent of P-H bond dissociation or ii) displacement of the PH_3 improper angle ($\angle$P-In-H$^-$), which is related to the phosphorus cone angle used to explain steric effects in catalysis[80], from that of the free precursor. A careful examination of the TS geometries reveals increases in P-H bond lengths but comparable cone angles (Supporting Information Table S5 and Figure S12). Thus, tuning the indium precursor favors a later transition state characterized by a longer P-H* bond (1.62 Å in acetate vs. 1.66 Å for trichloroacetate) due to formation of the In-P bond (2.61 Å in acetate vs. 2.57 Å in trichloracetate, see also Figure 4 and Supporting Information Table S5). We note that the difference in the cleaving P-H* and forming O-H* bonds with respect to bond distances provides a measure of reaction progress:

$$\delta = d_{\text{P-H*}} - d_{\text{H*-O}^-} \tag{2}$$

Thus, relative TS character, Δd, is best defined in terms of the difference of the individual

reaction progress metric, δ, in the ith TS compared to that in an acetate intracomplex TS reference ($d_{P\text{-}H^*}$=1.62 Å and $d_{H^*\text{-}O^-}$=1.34 Å):

$$\Delta d = \left(\frac{\delta_i^{TS} - \delta_{Ac,intra}^{TS}}{\delta_{Ac,intra}^{P} - \delta_{Ac,intra}^{TS}} \right) \times 100 \quad (3)$$

Computed values of Δd range from -2 to 10% for intracomplex transition states, where a negative value of Δd denotes an earlier TS, a positive value denotes a later TS, and 100% corresponds to the intracomplex product geometry ($d_{P\text{-}H^*}$=2.23 Å and $d_{H^*\text{-}O^-}$=1.00 Å). Nearly all functionalized indium precursors with later TSes (positive Δd) exhibit reduced E_a values. This apparent violation of Hammond-Leffler[81-82] is in fact reasonable and expected[83] due to the progress in In-P bond formation that drives down the activation energy for later TSes. This progress is revealed by the increasing interaction energies in the ASM analysis (Supporting Information Figure S13).

ASM analysis on intracomplex TSes has thus far suggested that increasing the strength of electron withdrawing substituents near the carboxylate should increase interaction energies in a later TS without substantially increasing the indium precursor strain energies. To confirm this hypothesis, we consider the propiolate ligand present in our data set that exhibits a slightly later TS and lower E_a compared to the acetate reference (E_a=18.4 kcal/mol, $E_{strain\text{-}In}$=39.9 kcal/mol, Δd=4.2%). The shift with respect to the acetate reference can be understood of the terms of the inductive effect, here increased due to hybridization of the *sp* carbon adjacent to the carbonyl. Although not present in our original data set, the cyanoformate ligand constructed by replacing the terminal alkyne carbon with a more electronegative nitrogen atom (pauling electronegativities χ_C = 2.25, χ_N = 3.04), contains an even stronger electron-withdrawing substituent. These linear substituents cannot readily form a sixth interaction with In and are sufficiently rigid to prevent inter-ligand hydrogen bond formation, isolating their role to case iii indirect effects on the carboxylate oxygen atoms. Indeed, the cyanoformate precursor exhibits a lower activation energy (E_a=13.7 kcal/mol) than any of the original 32 molecules studied

(Supporting Information Table S5).

ASM analysis on cyanoformate reveals a negligible increase in the indium strain energy to 40.5 kcal/mol and a significantly later transition state (Δd=11.4%, see also Supporting Information Table S6). Therefore, functionalization of the carboxylate ligands alters the electronic properties of the indium precursor by generally supporting an increasing geometric distortion in the indium and phosphorus precursors, as indicated by the later TS character, without an increased overall activation energetic penalty. These observations suggest that the carboxylate oxygen becomes a worse nucleophile with functionalization by electron-withdrawing groups, delaying formation of the O-H* bond. We quantified this effect by observing reduced values of the condensed Fukui functions[84-86] on the carboxylate oxygen from acetate to propiolate to cyanoformate or through increased halogenation (Supporting Information Text S1, Table S6, and Figure S14).

3d. Tuning Effects on Multi-Precursor Pathways

Having confirmed a correlation between In-O bond cleavage and intracomplex E_a reduction, we now turn to the lower energy and multi-precursor intercomplex pathway (Supporting Information Figure S15). For indium acetate, the intercomplex E_a is about 9 kcal/mol lower[42] than that for the intracomplex pathway. This lower activation energy is consistent with a later TS in the intercomplex pathway, as measured by a Δd of 9%, due to a 0.01 Å shorter In-P bond distance and 0.05 Å longer $H^{\cdot}$-O^{-} bond. We note this effect is not due to functionalization but a result of the looser geometric requirements when the acetate abstracting a proton from the phosphine is not the one forming the In-P bond.

ASM analysis on the indium acetate intercomplex TS confirms the E_a reduction is due to an increase in the magnitude of E_{int} by 12 kcal/mol, another indication of late TS character. Consistent with expectations of fewer constraints on the attacking geometry, the intercomplex pathway TS exhibits a slight reduction (3 kcal/mol) in phosphorus precursor strain energy despite an increase in the P-$H^{\cdot}$ distance that can be explained by a smaller displacement of the phosphine cone angle (Supporting Information Figure S12). The intercomplex In precursor strain

energy is increased by 6 kcal/mol over the intracomplex reference, despite our earlier hypothesis[42] that partial In-O bond cleavage (3.2 Å vs. 3.7 Å for intracomplex) in intercomplex pathways reduced In-P formation barriers. This modest $E_{strain\text{-}In}$ increase is due to the shift of the shared carboxylate between the two precursors from chelating bridging to standard bridging in the TS (Supporting Information Figure S15). Thus, additional strain arises from the distortion of two indium precursors in the intercomplex pathway, but this penalty is outweighed by stabilizing interactions and decreased distortion of the phosphorus precursor. Starting from a less stable bridging bidentate reactant or with larger indium clusters (e.g., trimers) would likely not alter trends in intercomplex E_a with functionalization but could likely reduce absolute barrier values.

Given the geometric differences of the intracomplex and intercomplex pathways, it is useful to verify that ligand-tuning effects observed for the former still hold for the latter, likely predominant pathway. Comparison of activation energies relative to respective indium acetate references (ΔE_a) upon functionalization reveals comparable tuning effects for the two pathways (Figure 5). In most cases, ΔE_a values are larger in magnitude for the intercomplex pathway, suggesting somewhat stronger tunability (Figure 5 and Supporting Information Table S7). Evaluation of our TS character heuristic, Δd, confirms this observation. The already later acetate intercomplex TS shows a wider spread ($8\% < \Delta d < 37\%$, Figure 6) upon functionalization than in the intracomplex cases ($-2\% < \Delta d < 10\%$). Activation energies for both pathways are well-correlated (R^2=0.84) to the Δd metric, with a 10% Δd increase projected to reduce the E_a by 5 kcal/mol (Figure 6). Increasingly favorable reaction energetics (E_{rxn}) with later TSes either from functionalization or from intracomplex to intercomplex pathways helps rationalize earlier observations of apparent violation of the Hammond-Leffler postulate[81-82] for both pathways (Figure 6 and Supporting Information Figures S16-S17). A reduction of the reaction energies by 2 kcal/mol is correlated to reductions in activation energies by 2.5 kcal/mol for the intracomplex pathway (Supporting Information Figure S16). There is more scatter in the relationship for the intercomplex pathway, with closer to a 1:1 relationship between the two quantities (Supporting

Information Figure S17).

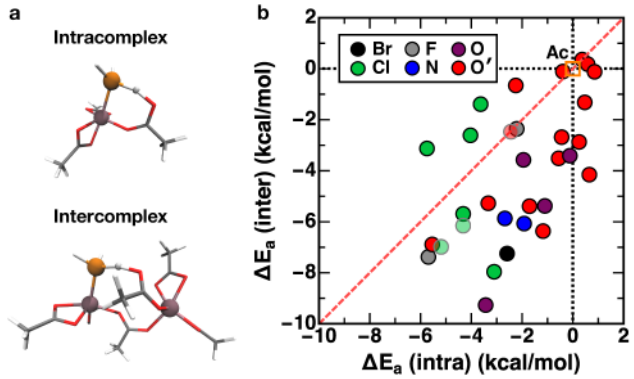

Figure 5. (a) TS structures of intracomplex (top) and intercomplex (bottom) pathways with $In(Ac)_3$ and one PH_3 molecule. Indium (brown) and phosphorus (orange) atoms are shown as spheres, whereas other atoms (oxygen in red, carbon in gray, and hydrogen in white) are shown in stick representation. (b) Relative E_a with respect to the $In(Ac)_3$ reference (empty orange square) for the intercomplex pathway versus the intracomplex pathway for 32 carboxylate ligands. The red diagonal line indicates parity between the pathways, and the black dotted vertical or horizontal line corresponds to no functionalization effect. Symbols with gray outlines have barrierless intercomplex pathway energetics, and the reaction enthalpy is used instead as a reference, as described in the main text.

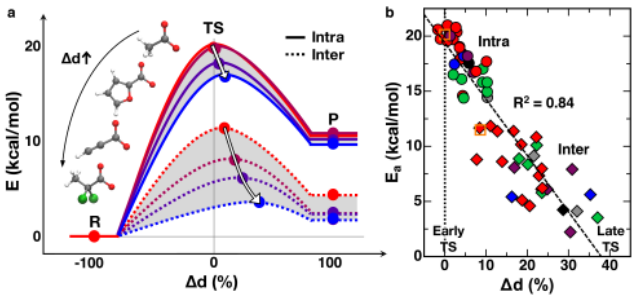

Figure 6. (a) In–P bond formation energetics of both the intracomplex (solid line) and intercomplex (dotted line) pathways for four indium precursors, $In(Ac)_3$ (red), $In(2\text{-furoate})_3$ (maroon), $In(propiolate)_3$ (purple) and $In(2,2\text{-dichloropropanoate})_3$ (blue). All atoms (oxygen in red, carbon in gray, chlorine in green, and hydrogen in white) are shown in ball-and-stick representation. The decrease in E_a with increasing Δd is indicated by a white arrow. (b) E_a (in kcal/mol) of both the intracomplex (circle) and intercomplex (diamond) pathways versus the corresponding TS structure parameter Δd (in %) relative to the intracomplex $In(Ac)_3$ TS (black dotted vertical line and empty orange square) with a best-fit line (black, dashed). Symbols are colored according to closest element in carboxylate to indium: Br (black), Cl (green), F (grey), N (blue), substituting O (maroon), or the original carboxylate, O', (red).

Returning to geometric origins of changes in both pathway TSes with functionalization, the TS does generally become more product-like, but the product reference, in which one In-O bond is traded for an In-P bond, is also becoming increasingly favorable. In fact, for the intercomplex

pathway α–trihalogenated carboxylates, the transition state character becomes so late that the reaction is essentially barrierless and a single transition state cannot be well-characterized. This energetic characteristic is not likely favorable for QD synthesis as reactions would become highly reversible. Instead, a balanced barrier reduction and equivalent tuning between the two pathways, which occurs for most of the complexes studied is likely preferable. We will revisit empirical strategies that can be used to identify candidate ligands in sec. 3e.

Analysis of the most tunable intercomplex structures reveals that the flexibility of the bridging acetate ligand (Figure 5a) can mediate both case ii (non-bonding In-ligand interactions) and case iii (indirect effects of ligand functionalization on In-O bonding) effects that were not possible in the intracomplex pathway. For instance, the 3-methyl-1,2,4-oxadiazole-5-carboxylate bridging ligand forms an additional short In-N interaction not present in the intracomplex pathway, resulting in an intercomplex pathway E_a reduction that is 5.8 kcal/mol larger than the intracomplex case (Supporting Information Table S7). In other cases (e.g., 4-hydroxy-2-butynoate), the intercomplex pathway is more tunable than the intracomplex pathway by 4-5 kcal/mol due to increased hydrogen-bonding interactions that stabilize the carboxylate oxygen atoms. Only a few cases correspond to less tuning in the intercomplex than intracomplex pathways (Figure 5). Comparison of ASM components of these 4 cases, which are typically monohalogenated at the α-carbon, reveals that the higher activation energy is due to higher indium precursor strain energies in the intercomplex case due to the shift of the bridging carboxylate in the TS without matching benefit in interaction energies.

ASM decomposition energies of all functionalized ligands in both the intracomplex and intercomplex mechanisms reveal consistent trends across the two pathways. In both cases, increasing interaction energies in functionalized precursors outpace moderately and weakly increasing strain energies in the phosphorus and indium precursors, respectively (Figure 7). Thus, for both pathways, functionalization increases In-P interaction strength with only weak increases in energetic penalty on the indium precursor (Supporting Information Figures S13 and S18). The

difference in transition state geometry yields different trendlines but comparable values of phosphorus strain for the two pathways (Figure 7). The indium precursor strain covers the narrowest range, suggesting that the effect of functionalization is to stabilize indium precursors to favor later TSes with limited, if any, energetic penalty for this further distortion that strengthens In-P bond formation in the TS. A clear correlation is observed in the phosphorus precursor strain energetics, conversely, because this strain arises from P-H bond stretching and cone angle distortion. If our definition of Δd is shifted by 9%, roughly the difference between the intercomplex and intracomplex acetate Δd values, the phosphorus precursor strain lines overlay exactly. This realignment is not necessary, however, for the interaction energies. The enhanced tuning for the intercomplex pathway in comparison to the intracomplex pathway in the majority of cases is likely due to the reduced indium precursor strain energies in comparison to the $In(Ac)_3$ intercomplex reference (see Figure 7). The few intercomplex cases with unusually negative interaction energies clustered (around -70 to -75 kcal/mol) around Δd=20% correspond to hydrogen bonding interactions formed in the intercomplex pathway between the two precursors that are mediated by the increased flexibility of the bridging indium precursors (Supporting Information Table S7 and associated structures).

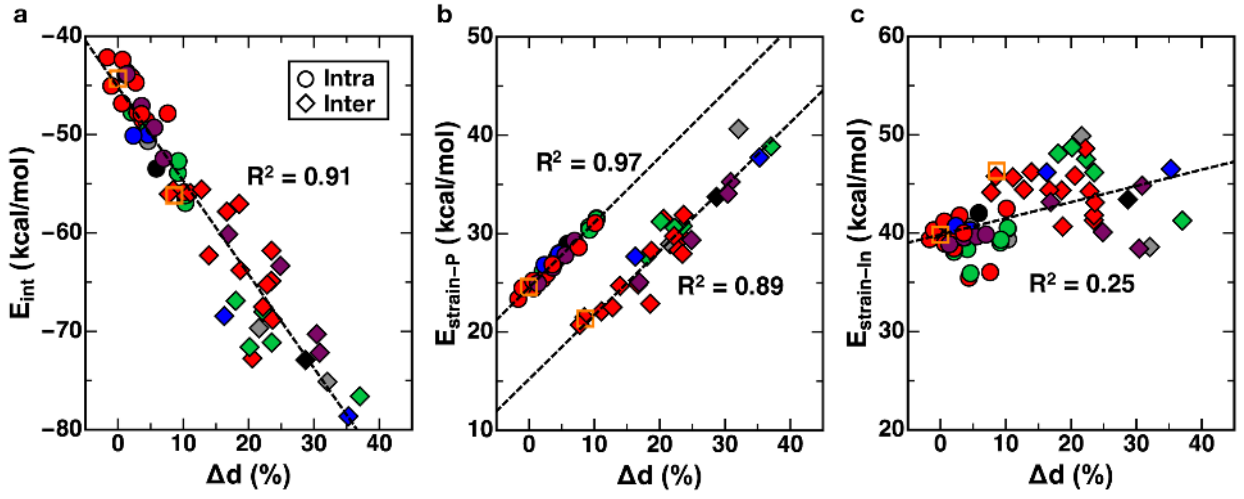

Figure 7. ASM energy components (in kcal/mol): a) interaction, b) phosphorus precursor strain, and c) indium precursor strain of both the intracomplex (circle) and intercomplex (diamond) pathways are shown as a function of the corresponding TS structure parameter Δd (in

%) relative to the intracomplex $In(Ac)_3$ TS. The black dashed lines indicate linear best-fit lines with correlation coefficients as shown. Symbols are colored according to closest element in carboxylate to indium: Br (black), Cl (green), F (grey), N (blue), substituting O (maroon), or the original carboxylate, O', (red).

3e. Preservation of Trends in Realistic Precursor Ligands

For efficiency in computational screening, we have focused on shorter chain indium precursors and smaller phosphorus precursors than are typically employed experimentally. To make a connection to realistic synthetic strategies, we now demonstrate the transferability of the observations of barrier tuning by chemical functionalization to larger systems and provide suggestions for a purely experimental approach to indium precursor selection.

Although phosphine has been occasionally employed experimentally[25, 87], the more commonly-employed phosphorus precursors for current InP QD synthesis recipes are tris(trimethylsilyl)phosphine ($P(SiMe_3)_3$, PTMS)[18, 20-21] and tris(trimethylgermyl)phosphine ($P(GeMe_3)_3$).[24] These two precursors are both much bulkier than phosphine. Additionally, whereas the P-H bond in phosphine is strongly covalent due to comparable substituent atom electronegativity (χ_P=2.19 and χ_H=2.20), P-Si and P-Ge bonds are more ionic due to lower electronegativities (χ_{Si}=1.90 and χ_{Ge}=2.01). In order to isolate any electronic effect of differing bond character (i.e., covalent P-H vs. ionic P-Si or P-Ge) on the phosphorus-ligand bond dissociation, we compare reactions of indium precursors with the simplified tris(silyl)phosphine ($P(SiH_3)_3$) and tris(germyl)phosphine ($P(GeH_3)_3$) ligands. These models provide comparable bond dissociation energies and partial charges of the P-X bond (X=Si, Ge) to the larger, methylated precursors (Supporting Information Table S8). The truncation from the full PTMS ligand is motivated by the difficulty associated with characterizing the transition state if the additional methyl groups are present.

We observe a comparable E_a of 21 kcal/mol for the phosphine and tris(trigermyl)phosphine precursors but a reduction in the activation energy to 15 kcal/mol for tris(trisilyl)phosphine precursors (Figure 8). The reduction in activation energy for the P-Si-bond-containing precursors

is consistent with both previous experimental study[26] and the low relative electronegativity of Si with respect to H and Ge. Most importantly, the trend of electron-withdrawing functionalization (e.g., with increasing chlorination) leading to a decrease in activation energy observed for phosphine is preserved (Figure 8). The comparable energetic trend with varying phosphorus precursor is also consistent with the previous TS character analysis carried out on phosphine (Supporting Information Text S2). Finally, the remarkable agreement between the energetics evaluated with P-H- and P-Ge-bond-containing precursors suggests that results on phosphine may be expected to hold both qualitatively and quantitatively for tris(trigermyl)- or tris(trimethylgermyl)-phosphine.

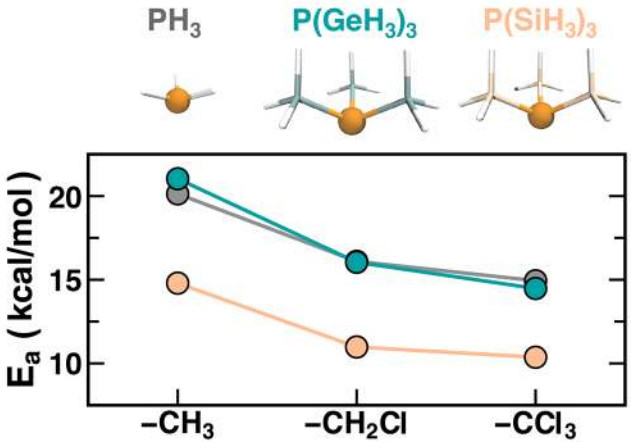

Figure 8. Activation energies (in kcal/mol) of intracomplex pathway for PH_3 (gray), $P(GeH_3)_3$ (teal) and $P(SiH_3)_3$ (pale orange) precursors each with three indium precursors, acetate (labeled -CH_3), chloroacetate, and trichloroacetate. Phosphorus (orange) atoms are shown as spheres, and other atoms (germanium in teal, silicon in pale orange, and hydrogen in white) are shown in stick representation (top).

For indium precursor chain length considerations, we revisit the commonly employed indium myristate ($In(My)_3$) precursor. We introduced functional groups at the α-carbon adjacent to the carboxylate based on our tuning observations (Supporting Information Figure S19). These functionalizations included: i) halogens (Br, Cl), ii) oxygen-containing OH and OCH_3, and iii) not-previously screened sulfur-containing SH and SCH_3. Methylated oxygen or sulfur groups were introduced as possible strategies to introduce a sixth interaction that was weaker than a

standard covalent bond, as flexible oxygen atoms had previously been observed to form too-short coordination in monodentate structures (see Sec. 3a). The large size and soft degrees of freedom in the long chains of the myristate-derivative ligands makes direct E_a calculation challenging, and so we focus on agreement of $\Delta E_{m\text{-}b}$ data. Overall, we observe good alignment of our functionalized $In(My)_3$ $\Delta E_{m\text{-}b}$ data with the previously calculated, small ligand trend with SCH_3 or Cl reducing the relative monodentate energy to around 12 kcal/mol from 19 kcal/mol for pristine $In(My)_3$ (see Supporting Information Figure S19). These observations suggest the general functional group trends unearthed for smaller molecules should be a suitable guide to functionalization of long-chain, experimentally employed precursors.

Our results thus far have revealed that less nucleophilic carboxylate oxygen anions produce later TSes with lower activation energies for In-P bond formation. Nucleophilicity can be estimated by the equilibrium constant for acid dissociation of the conjugate acid, i.e., the pK_a, with a lower pK_a corresponding to a weaker nucleophile for the conjugate base. pK_a values computed using empirical methods correlate well with both intracomplex and intercomplex In-P bond formation E_a values (Figure 9). There is slightly more scatter for the correlation with intracomplex energetics (R^2=0.42) versus intercomplex pathway (R^2=0.50). Scatter is likely due to neglect of interligand effects and approximations inherent in our use of semi-empirical pK_a estimation (see sec. 2). Scatter is generally comparable, even when only comparing ligands of the same closest-atom type (symbols in Fig. 9, see Supporting Information Figures S20-S21). Reduction of the carboxylic acid pK_a from the acetic acid reference by 1 unit is projected to reduce the intracomplex activation energies by around 1.1 kcal/mol, whereas the intercomplex pathway is reduced by 1.6 kcal/mol (equations provided in Supporting Information Text S3). This relationship holds for carboxylic acids with pK_as that are reduced due to substitution with electron withdrawing atoms or by unsaturation. Complexes of the conjugates bases of carboxylic acids with lower pK_as, such as tribromoacetic acid (pK_a = 0.71), 3-methyl-1,2,4-oxadiazole-5-carboxylic acid (pK_a = 0.19), and propiolic acid (pK_a=1.99), are calculated to have significantly lower activation energies (by ca. 5 kcal/mol) for both intracomplex and intercomplex pathways

than an acetic acid reference (Figure 9 and Supporting Information Tables S3, S5, and S7).

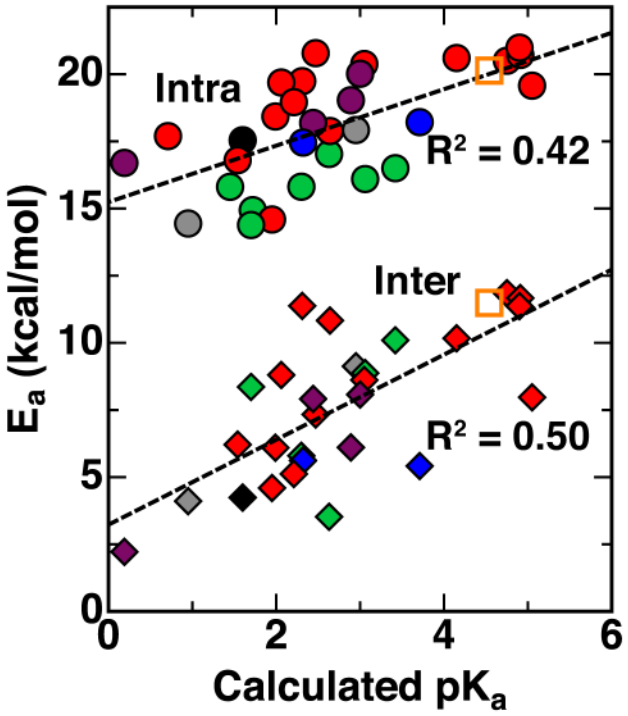

Figure 9. Activation energies (in kcal/mol) of both the intracomplex (circle) and intercomplex (diamond) pathways versus calculated pK_as of 32 carboxylate ligands with best-fit lines (black, dashed). Symbols are colored according to closest element in carboxylate to indium: Br (black), Cl (green), F (grey), N (blue), substituting O (maroon), or the original carboxylate, O', (red).

These observations support our use of shorter chain carboxylates in this study, as the experimental pK_a of myristic acid of 4.90 is quite close to that for acetic acid at 4.76.[88] Importantly, representative ligands that are calculated to alter growth kinetics through reduced pK_a do not appear to alter key electronic or optical properties (i.e., HOMO-LUMO gap) in a 1.3 nm InP QD model (Supporting Information Figure S22). Thus, we suggest an efficient means of selecting lab-appropriate precursors for InP QD synthesis: as long as they fit other design targets, use of more acidic (lower pK_a) carboxylic acids as ligands accelerates QD synthesis kinetics, thereby enabling lower temperature synthesis recipes that may enable better control of QD growth characteristics.

4. Conclusions

We have carried out a systematic screen of 210 diverse indium carboxylate precursors to

discover chemical functionalization that can tune In-O bond cleavage energetics critical in InP QD synthesis. We demonstrated the value of employing a large database normally used for discovery of drug-like molecules to discover design rules for inorganic complexes by maintaining realism (i.e., stable, synthetically accessible substituents) and providing diversity in functional groups. We confirmed a computationally efficient screening descriptor, the In-O bond cleavage energy, to be an excellent guide to candidates that lower In-P bond formation energetics for InP QD synthesis. The dominant factor in determining the In-O cleavage energetics was the presence of electron-withdrawing functional groups near the ligand carboxylate, although non-covalent interactions between the ligand and the In center also played a role.

Decomposition with the activation strain model revealed the source of transition-state stabilization in low activation energy carboxylates: increasing interaction between the precursors that corresponded to later TS character outweighed the increasing strain in the precursors. We rationalized the seeming violation of the Hammond-Leffler postulate of later TSes with lower activation energies by noting more favorable product energetics in those cases. Overall, weaker carboxylate oxygen nucleophiles favored stronger In-P bond formation in the TS, lowering activation energies. Extension to the multi-indium-precursor intercomplex pathway confirmed these observations. In fact, the higher flexibility in the bridging acetates of the intercomplex pathway often led to even greater stabilization.

Finally, we confirmed that our observations were unchanged across a range of phosphorus precursor chemistries (i.e., for P-H, P-Si, and P-Ge bonds) and in longer chain length carboxylates. Importantly, our observations of later TSes and weak nucleophiles lowering activation energies lead to a natural conclusion that the use of carboxylate ligands that are the conjugate bases of more acidic carboxylic acids will tune the kinetics of InP QD precursor synthesis. Thus, this computational study provides a new handle for InP QD synthesis that could lead to more controlled growth conditions to improve synthesized InP QD quality. Ongoing efforts in our lab are now focused on developing this general screening strategy for design of inorganic complexes to other critical areas of need.

ASSOCIATED CONTENT

Supporting Information. Structures of all monodentate and bidentate intermediates; details and chemdraws of ligand library screening set; flow chart of screening process; atomic mass and energetic correlations; example structures from screen; results of grafting study on monodentate-bidentate energetics; example structures of TS for intracomplex and intercomplex pathways; details of energetics (E_a and ASM energy components) and TS geometries ($d_{In\text{-}P}$, $d_{P\text{-}H}$, $d_{H\text{-}O}$, Δd and cone-angles) for intracomplex and intercomplex pathways; energetics and TS geometries correlations for intracomplex and intercomplex pathways including reaction energies; nucleophilic condensed Fukui function results; experimental pK_a of carboxylic acids; bond dissociation energies and partial charges of phosphorus precursors; activation energies with/without solvation effect or entropic contributions; comparison of LACVP* and aug-cc-pVTZ results; subgroup E_a-pK_a correlations; HOMO-LUMO gap of InP clusters. This material is available free of charge via the Internet at http://pubs.acs.org.

AUTHOR INFORMATION

Corresponding Author

*email: hjkulik@mit.edu phone: 617-253-4584

Notes

The authors declare no competing financial interest.

ACKNOWLEDGMENT

This work was supported by the National Science Foundation under grant number ECCS-1449291 (J.Y.K. and H.J.K) and an MIT Research Support Corporation Reed Grant (A.H.S). H.J.K. holds a Career Award at the Scientific Interface from the Burroughs Wellcome Fund. This work was carried out in part using computational resources from the Extreme Science and

Engineering Discovery Environment (XSEDE), which is supported by National Science Foundation grant number ACI-1053575.

REFERENCES

1. Talapin, D. V.; Lee, J.-S.; Kovalenko, M. V.; Shevchenko, E. V., Prospects of Colloidal Nanocrystals for Electronic and Optoelectronic Applications. *Chem. Rev.* **2010**, *110*, 389-458.
2. Alivisatos, A. P., Semiconductor Clusters, Nanocrystals, and Quantum Dots. *Science* **1996**, *271*, 933-937.
3. Semonin, O. E.; Luther, J. M.; Choi, S.; Chen, H.-Y.; Gao, J.; Nozik, A. J.; Beard, M. C., Peak External Photocurrent Quantum Efficiency Exceeding 100% via MEG in a Quantum Dot Solar Cell. *Science* **2011**, *334*, 1530-1533.
4. Kamat, P. V., Quantum Dot Solar Cells. Semiconductor Nanocrystals as Light Harvesters. *J. Phys. Chem. C* **2008**, *112*, 18737-18753.
5. Chuang, C.-H. M.; Brown, P. R.; Bulovic, V.; Bawendi, M. G., Improved Performance and Stability in Quantum Dot Solar Cells through Band Alignment Engineering. *Nat. Mater.* **2014**, *13*, 796-801.
6. Sun, Q.; Wang, Y. A.; Li, L. S.; Wang, D.; Zhu, T.; Xu, J.; Yang, C.; Li, Y., Bright, Multicoloured Light-Emitting Diodes Based on Quantum Dots. *Nat. Photonics* **2007**, *1*, 717-722.
7. Caruge, J. M.; Halpert, J. E.; Wood, V.; Bulovic, V.; Bawendi, M. G., Colloidal Quantum-Dot Light-Emitting Diodes with Metal-Oxide Charge Transport Layers. *Nat. Photonics* **2008**, *2*, 247-250.
8. Michalet, X.; Pinaud, F. F.; Bentolila, L. A.; Tsay, J. M.; Doose, S.; Li, J. J.; Sundaresan, G.; Wu, A. M.; Gambhir, S. S.; Weiss, S., Quantum Dots for Live Cells, in Vivo Imaging, and Diagnostics. *Science* **2005**, *307*, 538-544.
9. Parak, W. J.; Gerion, D.; Pellegrino, T.; Zanchet, D.; Micheel, C.; Williams, S. C.; Boudreau, R.; Le Gros, M. A.; Larabell, C. A.; Alivisatos, A. P., Biological Applications of Colloidal Nanocrystals. *Nanotechnology* **2003**, *14*, R15-R27.
10. Murray, C. B.; Norris, D. J.; Bawendi, M. G., Synthesis and Characterization of Nearly Monodisperse CdE (E = S, Se, Te) Semiconductor Nanocrystallites. *J. Am. Chem. Soc.* **1993**, *115*, 8706-8715.
11. Chen, O.; Zhao, J.; Chauhan, V. P.; Cui, J.; Wong, C.; Harris, D. K.; Wei, H.; Han, H. S.; Fukumura, D.; Jain, R. K., et al., Compact High-Quality CdSe-CdS Core-Shell Nanocrystals with Narrow Emission Linewidths and Suppressed Blinking. *Nat. Mater.* **2013**, *12*, 445-451.
12. Dabbousi, B. O.; RodriguezViejo, J.; Mikulec, F. V.; Heine, J. R.; Mattoussi, H.; Ober, R.; Jensen, K. F.; Bawendi, M. G., (CdSe)ZnS Core-Shell Quantum Dots: Synthesis and Characterization of a Size Series of Highly Luminescent Nanocrystallites. *J. Phys. Chem. B* **1997**, *101*, 9463-9475.
13. Kirchner, C.; Liedl, T.; Kudera, S.; Pellegrino, T.; Javier, A. M.; Gaub, H. E.; Stolzle, S.; Fertig, N.; Parak, W. J., Cytotoxicity of Colloidal CdSe and CdSe/ZnS Nanoparticles. *Nano Lett.* **2005**, *5*, 331-338.
14. Tamang, S.; Lincheneau, C.; Hermans, Y.; Jeong, S.; Reiss, P., Chemistry of InP Nanocrystal Syntheses. *Chem. Mater.* **2016**, *28*, 2491-2506.
15. Brunetti, V.; Chibli, H.; Fiammengo, R.; Galeone, A.; Malvindi, M. A.; Vecchio, G.; Cingolani, R.; Nadeau, J. L.; Pompa, P. P., InP/ZnS as a Safer Alternative to CdSe/ZnS Core/Shell Quantum Dots: In Vitro and in Vivo Toxicity Assessment. *Nanoscale* **2013**, *5*, 307-317.
16. Yang, X.; Zhao, D.; Leck, K. S.; Tan, S. T.; Tang, Y. X.; Zhao, J.; Demir, H. V.; Sun, X. W., Full Visible Range Covering InP/ZnS Nanocrystals with High Photometric Performance and Their Application to White Quantum Dot Light-Emitting Diodes. *Adv. Mater.* **2012**, *24*, 4180-4185.

17. Adam, S.; Talapin, D. V.; Borchert, H.; Lobo, A.; McGinley, C.; de Castro, A. R. B.; Haase, M.; Weller, H.; Moller, T., The Effect of Nanocrystal Surface Structure on the Luminescence Properties: Photoemission Study of Hf-Etched InP Nanocrystals. *J. Chem. Phys.* **2005**, *123*, 084706.
18. Baek, J.; Allen, P. M.; Bawendi, M. G.; Jensen, K. F., Investigation of Indium Phosphide Nanocrystal Synthesis Using a High-Temperature and High-Pressure Continuous Flow Microreactor. *Angew. Chem., Int. Ed.* **2011**, *50*, 627-630.
19. Gary, D. C.; Terban, M. W.; Billinge, S. J. L.; Cossairt, B. M., Two-Step Nucleation and Growth of InP Quantum Dots via Magic-Sized Cluster Intermediates. *Chem. Mater.* **2015**, *27*, 1432-1441.
20. Gary, D. C.; Cossairt, B. M., Role of Acid in Precursor Conversion During InP Quantum Dot Synthesis. *Chem. Mater.* **2013**, *25*, 2463-2469.
21. Gary, D. C.; Glassy, B. A.; Cossairt, B. M., Investigation of Indium Phosphide Quantum Dot Nucleation and Growth Utilizing Triarylsilylphosphine Precursors. *Chem. Mater.* **2014**, *26*, 1734-1744.
22. Xie, L.; Harris, D. K.; Bawendi, M. G.; Jensen, K. F., Effect of Trace Water on the Growth of Indium Phosphide Quantum Dots. *Chem. Mater.* **2015**, *27*, 5058-5063.
23. Allen, P. M.; Walker, B. J.; Bawendi, M. G., Mechanistic Insights into the Formation of InP Quantum Dots. *Angew. Chem., Int. Ed.* **2010**, *49*, 760-762.
24. Harris, D. K.; Bawendi, M. G., Improved Precursor Chemistry for the Synthesis of III-V Quantum Dots. *J. Am. Chem. Soc.* **2012**, *134*, 20211-20213.
25. Li, L.; Protière, M.; Reiss, P., Economic Synthesis of High Quality InP Nanocrystals Using Calcium Phosphide as the Phosphorus Precursor. *Chem. Mater.* **2008**, *20*, 2621-2623.
26. Franke, D.; Harris, D. K.; Xie, L.; Jensen, K. F.; Bawendi, M. G., The Unexpected Influence of Precursor Conversion Rate in the Synthesis of III-V Quantum Dots. *Angew. Chem., Int. Ed.* **2015**, *54*, 14299-14303.
27. Heath, J. R., Covalency in Semiconductor Quantum Dots. *Chem. Soc. Rev.* **1998**, *27*, 65-71.
28. Puzder, A.; Williamson, A. J.; Zaitseva, N.; Galli, G.; Manna, L.; Alivisatos, A. P., The Effect of Organic Ligand Binding on the Growth of CdSe Nanoparticles Probed by Ab Initio Calculations. *Nano Lett.* **2004**, *4*, 2361-2365.
29. Manna, L.; Wang, L.; Cingolani, R.; Alivisatos, A. P., First-Principles Modeling of Unpassivated and Surfactant-Passivated Bulk Facets of Wurtzite CdSe: A Model System for Studying the Anisotropic Growth of CdSe Nanocrystals. *J. Phys. Chem. B* **2005**, *109*, 6183-6192.
30. Hadley, A.; Aikens, C. M., Thiolate Ligand Exchange Mechanisms of Au1 and Subnanometer Gold Particle Au11. *J. Phys. Chem. C* **2010**, *114*, 18134-18138.
31. Fernando, A.; Aikens, C. M., Ligand Exchange Mechanism on Thiolate Monolayer Protected Au25(Sr)18 Nanoclusters. *J. Phys. Chem. C* **2015**, *119*, 20179-20187.
32. Barngrover, B. M.; Manges, T. J.; Aikens, C. M., Prediction of Nonradical Au(0)-Containing Precursors in Nanoparticle Growth Processes. *J. Phys. Chem. A* **2015**, *119*, 889-895.
33. Barngrover, B. M.; Aikens, C. M., The Golden Pathway to Thiolate-Stabilized Nanoparticles: Following the Formation of Gold(I) Thiolate from Gold(III) Chloride. *J. Am. Chem. Soc.* **2012**, *134*, 12590-12595.
34. Zhao, Q.; Xie, L.; Kulik, H. J., Discovering Amorphous Indium Phosphide Nanostructures with High-Temperature Ab Initio Molecular Dynamics. *J. Phys. Chem. C* **2015**, *119*, 23238-23249.
35. Wood, B. C.; Ogitsu, T.; Schwegler, E., Local Structural Models of Complex Oxygen- and Hydroxyl-Rich GaP/InP(001) Surfaces. *J. Chem. Phys.* **2012**, *136*, 064705.
36. Wood, B. C.; Schwegler, E.; Choi, W. I.; Ogitsu, T., Hydrogen-Bond Dynamics of Water at the Interface with InP/GaP(001) and the Implications for Photoelectrochemistry. *J. Am. Chem. Soc.* **2013**, *135*, 15774-15783.
37. Wood, B. C.; Schwegler, E.; Choi, W. I.; Ogitsu, T., Surface Chemistry of GaP(001) and InP(001) in Contact with Water. *J. Phys. Chem. C* **2014**, *118*, 1062-1070.

38. Roy, S.; Springborg, M., Theoretical Study of Structural and Electronic Properties of Naked Stoichiometric and Nonstoichiometric Indium Phosphide Clusters. *J. Phys. Chem. B* **2003**, *107*, 2771-2779.
39. Roy, S.; Springborg, M., Theoretical Investigation of the Influence of Ligands on Structural and Electronic Properties of Indium Phosphide Clusters. *J. Phys. Chem. A* **2005**, *109*, 1324-1329.
40. Eunseog, C.; Hyosook, J.; Junho, L.; Eunjoo, J., Modeling on the Size Dependent Properties of InP Quantum Dots: A Hybrid Functional Study. *Nanotechnology* **2013**, *24*, 215201.
41. Zhao, Q.; Ng, S. S. H.; Kulik, H. J., Predicting the Stability of Fullerene Allotropes Throughout the Periodic Table. *J. Phys. Chem. C* **2016**, *120*, 17035-17045.
42. Xie, L.; Zhao, Q.; Jensen, K. F.; Kulik, H. J., Direct Observation of Early-Stage Quantum Dot Growth Mechanisms with High-Temperature Ab Initio Molecular Dynamics. *J. Phys. Chem. C* **2016**, *120*, 2472-2483.
43. Cossairt, B. M., Shining Light on Indium Phosphide Quantum Dots: Understanding the Interplay among Precursor Conversion, Nucleation, and Growth. *Chem. Mater.* **2016**, *28*, 7181-7189.
44. Gary, D. C.; Flowers, S. E.; Kaminsky, W.; Petrone, A.; Li, X.; Cossairt, B. M., Single-Crystal and Electronic Structure of a 1.3 Nm Indium Phosphide Nanocluster. *J. Am. Chem. Soc.* **2016**, *138*, 1510-1513.
45. Green, M.; O'Brien, P., A Novel Metalorganic Route for the Direct and Rapid Synthesis of Monodispersed Quantum Dots of Indium Phosphide. *Chem. Commun.* **1998**, 2459-2460.
46. Liu, Z.; Kumbhar, A.; Xu, D.; Zhang, J.; Sun, Z.; Fang, J., Coreduction Colloidal Synthesis of III-V Nanocrystals: The Case of InP. *Angew. Chem., Int. Ed.* **2008**, *47*, 3540-3542.
47. Jun, K.-W.; Khanna, P. K.; Hong, K.-B.; Baeg, J.-O.; Suh, Y.-D., Synthesis of InP Nanocrystals from Indium Chloride and Sodium Phosphide by Solution Route. *Mater. Chem. Phys.* **2006**, *96*, 494-497.
48. Battaglia, D.; Peng, X., Formation of High Quality InP and InAs Nanocrystals in a Noncoordinating Solvent. *Nano Lett.* **2002**, *2*, 1027-1030.
49. Tessier, M. D.; De Nolf, K.; Dupont, D.; Sinnaeve, D.; De Roo, J.; Hens, Z., Aminophosphines: A Double Role in the Synthesis of Colloidal Indium Phosphide Quantum Dots. *J. Am. Chem. Soc.* **2016**, *138*, 5923-5929.
50. Lucey, D. W.; MacRae, D. J.; Furis, M.; Sahoo, Y.; Cartwright, A. N.; Prasad, P. N., Monodispersed InP Quantum Dots Prepared by Colloidal Chemistry in a Noncoordinating Solvent. *Chem. Mater.* **2005**, *17*, 3754-3762.
51. Xu, S.; Kumar, S.; Nann, T., Rapid Synthesis of High-Quality InP Nanocrystals. *J. Am. Chem. Soc.* **2006**, *128*, 1054-1055.
52. Cros-Gagneux, A.; Delpech, F.; Nayral, C.; Cornejo, A.; Coppel, Y.; Chaudret, B., Surface Chemistry of InP Quantum Dots: A Comprehensive Study. *J. Am. Chem. Soc.* **2010**, *132*, 18147-18157.
53. Gaulton, A.; Bellis, L. J.; Bento, A. P.; Chambers, J.; Davies, M.; Hersey, A.; Light, Y.; McGlinchey, S.; Michalovich, D.; Al-Lazikani, B., et al., Chembl: A Large-Scale Bioactivity Database for Drug Discovery. *Nucleic Acids Res.* **2012**, *40*, D1100-D1107.
54. Ioannidis, E. I.; Gani, T. Z.; Kulik, H. J., Molsimplify: A Toolkit for Automating Discovery in Inorganic Chemistry. *J. Comput. Chem.* **2016**, *37*, 2106-2117.
55. Hansen, E. C.; Pedro, D. J.; Wotal, A. C.; Gower, N. J.; Nelson, J. D.; Caron, S.; Weix, D. J., New Ligands for Nickel Catalysis from Diverse Pharmaceutical Heterocycle Libraries. *Nat. Chem.* **2016**, *8*, 1126-1130.
56. Lee, C.; Yang, W.; Parr, R. G., Development of the Colle-Salvetti Correlation-Energy Formula into a Functional of the Electron Density. *Phys. Rev. B* **1988**, *37*, 785-789.
57. Becke, A. D., Density-Functional Thermochemistry. III. The Role of Exact Exchange. *J. Chem. Phys.* **1993**, *98*, 5648-5652.

58. Stephens, P. J.; Devlin, F. J.; Chabalowski, C. F.; Frisch, M. J., Ab Initio Calculation of Vibrational Absorption and Circular Dichroism Spectra Using Density Functional Force Fields. *J. Phys. Chem.* **1994**, *98*, 11623-11627.
59. Vosko, S. H.; Wilk, L.; Nusair, M., Accurate Spin-Dependent Electron Liquid Correlation Energies for Local Spin Density Calculations: A Critical Analysis. *Can. J. Phys.* **1980**, *58*, 1200-1211.
60. Ufimtsev, I. S.; Martinez, T. J., Quantum Chemistry on Graphical Processing Units. 3. Analytical Energy Gradients, Geometry Optimization, and First Principles Molecular Dynamics. *J. Chem. Theory Comput.* **2009**, *5*, 2619-2628.
61. Petachem. http://www.petachem.com. (accessed November 13, 2016).
62. Hay, P. J.; Wadt, W. R., Abinitio Effective Core Potentials for Molecular Calculations - Potentials for the Transition-Metal Atoms Sc to Hg. *J. Chem. Phys.* **1985**, *82*, 270-283.
63. Kästner, J.; Carr, J. M.; Keal, T. W.; Thiel, W.; Wander, A.; Sherwood, P., DL-FIND: An Open-Source Geometry Optimizer for Atomistic Simulations†. *J. Phys. Chem. A* **2009**, *113*, 11856-11865.
64. Gani, T. Z. H.; Ioannidis, E. I.; Kulik, H. J., Computational Discovery of Hydrogen Bond Design Rules for Electrochemical Ion Separation. *Chem. Mater.* **2016**, *28*, 6207-6218.
65. Henkelman, G.; Jonsson, H., Improved Tangent Estimate in the Nudged Elastic Band Method for Finding Minimum Energy Paths and Saddle Points. *J. Chem. Phys.* **2000**, *113*, 9978-9985.
66. Henkelman, G.; Uberuaga, B. P.; Jonsson, H., A Climbing Image Nudged Elastic Band Method for Finding Saddle Points and Minimum Energy Paths. *J. Chem. Phys.* **2000**, *113*, 9901-9904.
67. Baker, J., An Algorithm for the Location of Transition-States. *J. Comput. Chem.* **1986**, *7*, 385-395.
68. Shao, Y.; Molnar, L. F.; Jung, Y.; Kussmann, J.; Ochsenfeld, C.; Brown, S. T.; Gilbert, A. T. B.; Slipchenko, L. V.; Levchenko, S. V.; O'Neill, D. P., et al., Advances in Methods and Algorithms in a Modern Quantum Chemistry Program Package. *Phys. Chem. Chem. Phys.* **2006**, *8*, 3172-3191.
69. Marvinsketch (17.1.19.0), 2016, Chemaxon. http://www.chemaxon.com (accessed February 2, 2017).
70. Xie, L.; Shen, Y.; Franke, D.; Sebastian, V.; Bawendi, M. G.; Jensen, K. F., Characterization of Indium Phosphide Quantum Dot Growth Intermediates Using Maldi-Tof Mass Spectrometry. *J. Am. Chem. Soc.* **2016**, *138*, 13469-13472.
71. Bender, A.; Glen, R. C., Molecular Similarity: A Key Technique in Molecular Informatics. *Org. Biomol. Chem.* **2004**, *2*, 3204-3218.
72. Eckert, H.; Bojorath, J., Molecular Similarity Analysis in Virtual Screening: Foundations, Limitations and Novel Approaches. *Drug Discovery Today* **2007**, *12*, 225-233.
73. Fernandez, I.; Bickelhaupt, F. M., The Activation Strain Model and Molecular Orbital Theory: Understanding and Designing Chemical Reactions. *Chem. Soc. Rev.* **2014**, *43*, 4953-4967.
74. van Zeist, W. J.; Bickelhaupt, F. M., The Activation Strain Model of Chemical Reactivity. *Org. Biomol. Chem.* **2010**, *8*, 3118-3127.
75. Diefenbach, A.; Bickelhaupt, F. M., Activation of H-H, C-H, C-C, and C-Cl Bonds by Pd(0). Insight from the Activation Strain Model. *J. Phys. Chem. A* **2004**, *108*, 8460-8466.
76. Fackler, P.; Huber, S. M.; Bach, T., Enantio- and Regioselective Epoxidation of Olefinic Double Bonds in Quinolones, Pyridones, and Amides Catalyzed by a Ruthenium Porphyrin Catalyst with a Hydrogen Bonding Site. *J. Am. Chem. Soc.* **2012**, *134*, 12869-12878.
77. Green, A. G.; Liu, P.; Merlic, C. A.; Houk, K. N., Distortion/Interaction Analysis Reveals the Origins of Selectivities in Iridium-Catalyzed C-H Borylation of Substituted Arenes and 5-Membered Heterocycles. *J. Am. Chem. Soc.* **2014**, *136*, 4575-4583.
78. Yu, P.; Yang, Z.; Liang, Y.; Hong, X.; Li, Y.; Houk, K. N., Distortion-Controlled Reactivity and Molecular Dynamics of Dehydro-Diels-Alder Reactions. *J. Am. Chem. Soc.* **2016**, *138*, 8247-8252.

79. Liu, F.; Paton, R. S.; Kim, S.; Liang, Y.; Houk, K. N., Diels-Alder Reactivities of Strained and Unstrained Cycloalkenes with Normal and Inverse-Electron-Demand Dienes: Activation Barriers and Distortion/Interaction Analysis. *J. Am. Chem. Soc.* **2013,** *135*, 15642-15649.
80. Tolman, C. A., Steric Effects of Phosphorus Ligands in Organometallic Chemistry and Homogeneous Catalysis. *Chem. Rev.* **1977,** *77*, 313-348.
81. Hammond, G. S., A Correlation of Reaction Rates. *J. Am. Chem. Soc.* **1955,** *77*, 334-338.
82. Leffler, J. E., Parameters for the Description of Transition States. *Science* **1953,** *117*, 340-341.
83. Farcasiu, D., The Use and Misuse of the Hammond Postulate. *J. Chem. Ed.* **1975,** *52*, 76-79.
84. Parr, R. G.; Yang, W., Density Functional Approach to the Frontier-Electron Theory of Chemical Reactivity. *J. Am. Chem. Soc.* **1984,** *106*, 4049-4050.
85. Fukui, K., Role of Frontier Orbitals in Chemical Reactions. *Science* **1982,** *218*, 747-754.
86. Yang, W.; Mortier, W. J., The Use of Global and Local Molecular Parameters for the Analysis of the Gas-Phase Basicity of Amines. *J. Am. Chem. Soc.* **1986,** *108*, 5708-5711.
87. Lim, T. H.; Ravi, S.; Bumby, C. W.; Etchegoin, P. G.; Tilley, R. D., Synthesis, Characterization and Photoconductivity of Highly Crystalline InP Nanowires Prepared from Solid Hydrogen Phosphide. *J. Mater. Chem.* **2009,** *19*, 4852-4856.
88. Barratt, M., Quantitative Structure-Activity Relationships (QSARs) for Skin Corrosivity of Organic Acids, Bases and Phenols: Principal Components and Neural Network Analysis of Extended Datasets. *Toxicol. In Vitro* **1996,** *10*, 85-94.

TOC Graphic